Attenuation Compensation in Single-Photon Emission Tomography: A Comparative Evaluation

Margaret H. Lewis, James T. Willerson, Samuel E. Lewis, Frederick J. Bonte, Robert W. Parkey, and Ernest M. Stokely

The University of Texas Health Science Center at Dallas, Dallas, Texas

Attenuation of photons in single-photon emission tomography (SPECT) makes three-dimensional reconstruction of unknown radioactivity distributions a mathematically intractable problem. Approaches to approximate SPECT reconstruction range from ignoring the effects of photon attenuation to incorporating assumed attenuation coefficients into an iterative reconstruction procedure. We have developed a computer-based simulation method to assess the relative effectiveness of attenuation compensation procedures. The method was used to study four procedures for myocardial SPECT using an infarct-avid radiopharmaceutical, Tc-99m stannous pyrophosphate. Reconstructions were evaluated by two criteria: overall (sum-of-squares) accuracy, and accuracy of lesion sizing. For moderate- to high-contrast studies there were no significant differences among the reconstructions by either evaluation criterion; for low contrast ratios the iterative method produced lower sum-of-squares error. We conclude that the additional expense of the iterative method is not justified under the conditions of this study. The approach used here is a convenient tool for evaluating specific SPECT reconstruction alternatives.

J Nucl Med 23: 1121–1127, 1982

Single-photon emission tomography (SPECT) provides a method for reconstructing the three-dimensional distribution of a radioactive tracer in the body using readily available radionuclides such as technetium-99m with a rotating gamma camera or multi-detector system. Unlike transmission tomography, SPECT involves determination of unknown source activity in the presence of unknown tissue attenuation, a problem that has no analytical solution (*1*,*2*). There are three approaches to approximate solutions of the SPECT reconstruction problem:

1. Attenuation may be ignored, which results in a reconstruction of "attenuated source" activity. This approach has been used for qualitative clinical studies but may not be adequate for quantitative studies (*3*,*4*).

2. Simplifying assumptions about attenuation—for example, that the attenuating tissue has uniform density and a known shape—may be incorporated into the reconstruction. These assumptions reduce the mathematical difficulty of the reconstruction problem, but may be inadaequate in real situations. Several investigators have developed SPECT reconstruction methods of this type (*1*,*5–15*).

3. A separate transmission CT procedure may be used to determine attenuation coefficients; this provides *a priori* information for the reconstruction of source activity. This approach has been implemented with iterative reconstruction techniques (*14*,*15*).

SPECT has important potential for noninvasive assessment of physiological function at low relative cost, but the limitations and strengths of the reconstruction methods used must be understood if reliable quantitative results are desired. The present study used computer-based simulation to investigate the relative effectiveness of four methods of attenuation compensation for myo-

Received Jan. 6, 1982; revision accepted Aug. 23, 1982.

For reprints contact: Dr. Margaret Lewis, Dept. of Radiology, The University of Texas Health Science Center at Dallas, 5323 Harry Hines Blvd., Dallas, TX 75235.

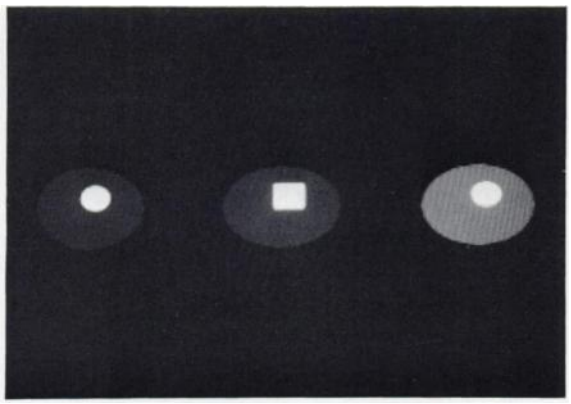

FIG. 1. Sum-of-squares error (SSE) may be misleading. Using left-hand figure as reference, SSE for right-hand figure is larger than that for the middle one, although shapes and locations in right-hand figure are identical to those in the reference.

cardial imaging using infarct-avid radionuclides. The general approach developed for this study would provide a convenient mechanism for assessment of other SPECT protocols as well.

EVALUATION OF ECT RECONSTRUCTION

It is difficult to evaluate a tomographic reconstruction: a "correct" image is generally not available, and there are conflicting criteria by which accuracy can be measured. One accuracy measure, used previously to compare tomographic reconstruction methods (*15,16*), relates an estimated (reconstructed) image to a reference ("correct") image using a sum-of-squares error calculation (SSE) given by:

$$SSE = \sum_{i=1}^{N} \frac{(m_i - p_i)^2}{(m_i - \bar{m})^2},$$

where N = number of pixels in the image (or number of pixels in a region of interest),

p_i = i^{th} pixel value in estimated image,
m_i = i^{th} pixel value in reference image, and
$\bar{m}$ = mean pixel value in reference image.

Although the SSE value reflects overall pixel-by-pixel reconstruction accuracy, this measure does not necessarily indicate whether a particular object in the image can be detected or located accurately. For example, a reconstructed image could contain a geometrically accurate lesion but with contrast different from the original; in this case the SSE value could be large, but the reconstruction may be clinically useful (Fig. 1).

The SSE is a poor evaluation measure if the goal of the tomographic study is lesion definition rather than overall reconstruction accuracy. This situation occurs with myocardial imaging using technetium-99m stannous pyrophosphate (Tc-99m PPi), an agent that concentrates in infarcted myocardial tissue (*17,18*). The extent of myocardial damage is defined by the infarct boundaries rather than by absolute activity levels in a Tc-99m PPi image (*19,20*); thus, an attenuation-compensation procedure that produces improved image contrast at the expense of distorted region boundaries would not improve the ability to quantitate Tc-99m PPi images.

We compared the relative capabilities of the three approaches to SPECT reconstruction of myocardial infarction imaged with Tc-99m PPi, using both accuracy of lesion definition and SSE as evaluation criteria. With computer-based simulation, we simulated a variety of clinical situations.

DESIGN OF STUDY

A. The simulation model. A general cross-sectional model of the human thorax was designed, including chest outline, lungs, heart, sternum, ribs, and vertebrae. Three types of myocardial infarction (MI) were added to the model: anterolateral transmural, subendocardial, and inferior lesions. For this study, source activity levels were based on the properties of Tc-99m PPi, which localizes in infarct and bone (Fig. 2, top). MI-to-background activity ratios of 3:1, 5:1, and 9:1 were used, representing a clinically realistic range of image contrasts. Attenuation levels were assigned for the 140-keV photons of Tc-99m (*21*): μ = 0.147/cm for soft tissue, 0.052/cm for lungs, and 0.259/cm for bone. A support table was incorporated in the model, having no source activity but providing attenuation characteristics equal to that of bone (Fig. 2, bottom). Data acquisition was simulated for a rotating gamma-camera system,* according to protocols used by other investigators (*22,23*). Projection raysums were calculated analytically from the model's geometry for 64 and 128 equally spaced angles over 360°; 64 projection bins of length 0.625 cm produced a total length of 40 cm per projection. Poisson noise was

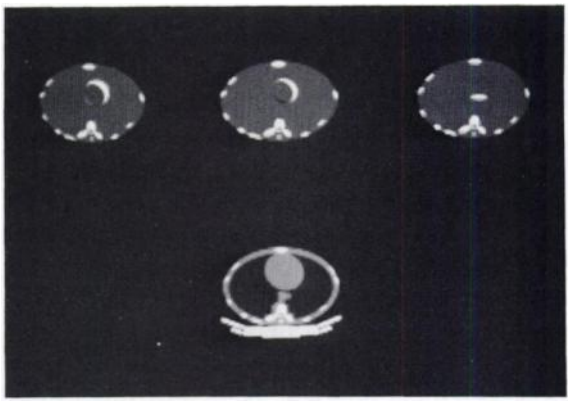

FIG. 2. Top: Activity distributions of cross-sectional thorax model. Lightest regions correspond to highest radionuclide activity. Three infarct geometries are, from left to right: anterolateral transmural, subendocardial, and inferior. Bottom: Attenuation distribution of model. Lightest regions correspond to greatest attenuation values. Note support table, which provides attenuation without activity.

added to each projection to produce three studies having 50K, 100K, and 200K total counts for each model specification. Thus for each of the three MI geometries, eighteen scanning situations were simulated, incorporating three MI-to-background activity ratios, two angular configurations, and three levels of count statistics. Each of the 54 simulated tomographic studies was reconstructed using four reconstruction methods with a general tomographic software package (*24*) that we modified to include reconstruction methods B and C below.

B. Reconstruction methods. Four reconstruction methods were evaluated. The first method ignored attenuation, two methods compensated for assumed uniform attenuation using simple techniques, and one method compensated for variable attenuation by an iterative technique with assumed attenuation distribution. Correct values for attenuation coefficients and body contours were used. The four methods, A, B, C, and D, are as follows:

Method A. Filtered back-projection method. One-dimensional convolution of the projection data was performed before back-projecting, using the Shepp-Logan convolution function (*25*). In frequency space this convolution is equivalent to the ramp function multiplied by the "sinc" window (*26*):

$$W(f) = \begin{cases} \dfrac{\sin(\pi f/f_n)}{(\pi f/f_n)} & \text{for } |f| \le f_n \\ 0, & \text{elsewhere,} \end{cases}$$

where f_n is the cutoff frequency.

Method B. Exponential raysum-combining method (*15*). This used reconstruction method A with a set of modified projection values based on the arithmetic mean of opposing projection raysums:

$$p_{new} = \frac{2(p_a + p_b)}{1 + 2e^{-x} + e^{-2x}}$$

where

p_{new} = modified projection,
$x = \mu L/2$,
μ = uniform attenuation coefficient (0.147/cm was used),
L = length of path through attenuating medium,
p_a = one projection bin value,
p_b = opposite projection bin value.

Method C. Geometric-mean corrector (*15*). This method used reconstruction method A with modified projection values based on the geometric mean of opposing raysums and a hyperbolic-sine corrector:

$$p_{new} = \frac{xe^x \sqrt{p_a p_b}}{\sinh(x)},$$

with parameters as above.

Method D. Iterative least-squares method (*14,15*), which used an iterative method to minimize the function

$$X^2 = \sum_{km} \sum_{ij} (F_{ij}^{km} X_{ij} - p_{km})^2$$

where

p_{km} = measured projection at bin k, angle m,
X_{ij} = intensity of pixel ij,
F_{ij}^{km} = fraction of pixel ij that projects into p_{km}.

Attenuation was incorporated into the reconstruction from the attenuation distribution A_{ij}^{km} by:

$$p_{km} = \sum_{ij} F_{ij}^{km} A_{ij}^{km} X_{ij}.$$

Minimization was done using the gradient technique, or method of steepest descent, with parameter scaling to speed convergence (*24*).

Although other methods for uniform attenuation compensation (e.g., *8*, *11*, *12*) may produce more accurate results than compensation methods B and C, the intent of this study was to investigate relative performance of the simplest currently used algorithms† compared with the theoretically most accurate (*15*) attenuation compensation algorithm. Each simulated set of projections was reconstructed by each of the four methods, and the resulting images were stored as 64 × 64 image matrices. Reconstruction times for the 64-projection studies were 24 sec for method A; 1 min for methods B and C; and 14 min 28 sec for method C. The 128-projection studies took approximately twice as long to reconstruct‡.

C. Evaluation parameters. Each image was analyzed automatically within a selected region using an empirically determined threshold setting. For each of the three MI geometries, a region of interest (ROI) was selected to contain the infarct near the center of the ROI. Each ROI reconstruction image was smoothed (unweighted 9-point smoothing) and its pixel values were scaled to the same range (values 0-255). All regions of contiguous pixels having values greater than a heuristically determined threshold (value 160) were identified, and the region closest to the center of the ROI was selected as the "lesion". The lesion size was recorded as the number of pixels in the lesion.

In addition, SSE values were calculated for each of the reconstructed images, using the same ROI as that used for lesion sizing and using the "correct" simulated activity model for the reference image. Both reconstructed and reference ROI images were smoothed and scaled, as above, before calculation of the SSE value.

RESULTS

Lesion sizes for the simulated MI models were: 21 to 36 pixels for the anterolateral infarcts, 21 to 41 pixels for

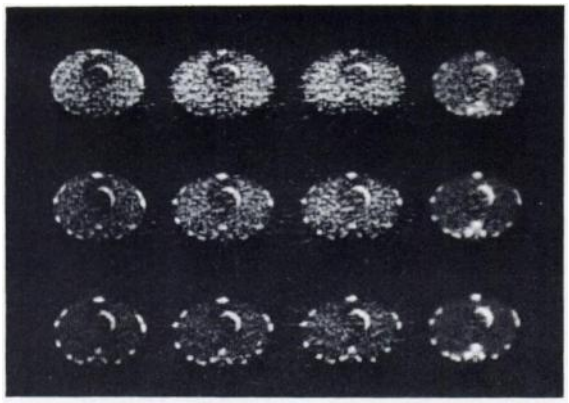

FIG. 3. Anterolateral MI reconstructions for 64-projection 100,000-count studies. MI-to-background activity ratios are, from top to bottom, 3:1, 5:1, and 9:1. Reconstruction methods used were, from left to right, methods A, B, C, and D as described in text.

the subendocardial infarcts, and 14 to 18 pixels for the inferior infarcts, depending on MI-to-background ratios. The varying model sizes for different MI-to-background contrasts indicate the effects of averaging during digitization, and of using a single threshold for lesion detection. Reconstructed lesion sizes ranged from 13 to 114 pixels for anterolateral, 5 to 124 pixels for subendocardial, and 7 to 120 pixels for the inferior lesion model. Increased MI-to-background contrast improved the reconstructions, as illustrated in Fig. 3. Increased counts generally improved the reconstructions, as indicated in Table 1. For eight of the 12 comparisons of Table 1, SSE improved as total counts increased; three of the remaining four showed less than 10% deviation from this pattern.

The results of six reconstructions—using 64 and 128 projections and using 50K, 100K, and 200K counts—were averaged for each reconstruction method to provide a statistical comparison of methods for each infarct geometry and contrast ratio. Results for both lesion size and SSE are given in Table 2 and in Figs. 4 and 5. By both lesion-size and SSE criteria, reconstruction accuracy improved as MI-to-background contrast increased for all infarct geometries and reconstruction methods. Using rank 1 for the best and rank 4 for the worst, the average ranks of the four reconstruction methods according to lesion size were: method A, 1.89; B, 2.06; C, 3.22; and D, 2.83. Ranking by SSE, the average ranks were: method A, 3.33; B, 1.89, C, 2.66; and D, 2.11. With all contrast ratios and MI geometries considered together, differences in the four methods were marginally significant statistically, $p < 0.10$, according to both lesion size and SSE (Friedman two-way analysis of variance, *27*). Method D produced the best reconstructions in SSE sense ($p < 0.02$) for the inferior lesions. For the anterolateral and subendocardial MIs and activity ratios of 5:1 or greater, method A outperformed method D with respect to lesion sizing ($p < 0.05$). However, no method gave significantly better results for any single infarct model according to the lesion-size criterion for all contrast ratios.

DISCUSSION

The simulation models of the present study did not incorporate organ motion; thus the reconstructions of the heart region from this study are better than those obtainable with a beating heart. It is likely, however, that performance of the four methods would be affected similarly by organ motion. In addition, we used higher values for table attenuation than may be needed in the clinical setting, and this could produce unrealistically poor reconstructions. Repeating some of the simulations with a 50% reduction in table attenuation, we found that lesion sizes and SSE values for the region of the heart were essentially unchanged; smaller table attenuation did lead to improved visualization of vertebral structure in the reconstructions. The simulation study also omitted

TABLE 1. EFFECT OF PHOTON STATISTICS ON SSE RECONSTRUCTION ACCURACY

Lesion type	No. counts in study	SSE for reconstruction method*			
		A	B	C	D
Anterolateral	50,000	.26	.19	.26	.71
	100,000	.17	.11	.16	.28
	200,000	.17	.08	.10	.12
Subendocardial	50,000	.56	.39	.41	.35
	100,000	.22	.20	.42	.38
	200,000	.32	.17	.19	.16
Inferior	50,000	.90	.81	.80	.15
	100,000	.66	.54	.50	.10
	200,000	.58	.53	.52	.06

* Calculated sum-of-squares error values for 64-projection studies with 5:1 MI-to-background contrast.

TABLE 2. LESION-SIZE AND SSE RESULTS FROM RECONSTRUCTION METHODS

		Actual	Lesion sizes in pixels (mean ± s.e.m., N = 6)*				SSE (mean ± s.e.m., N = 6)*			
			A	B	C	D	A	B	C	D
Anterior lesion	3:1	36	41.8 ± 12.2	46.8 ± 14.7	53.2 ± 14.0	45.5 ± 3.5	.93 ± .17	.56 ± .12	.51 ± .08	.38 ± .06
	5:1	26	24.2 ± 1.2	26.8 ± 1.1	29.0 ± 1.0	35.0 ± 2.2	.21 ± .03	.13 ± .02	.18 ± .03	.26 ± .04
	9:1	21	18.7 ± 1.2	20.5 ± 1.0	22.2 ± 0.9	29.2 ± 2.0	.07 ± .01	.05 ± .01	.08 ± .01	.16 ± .01
Subendocardial Lesion	3:1	41	22.7 ± 12.3	78.8 ± 12.0	98.5 ± 10.9	71.2 ± 8.4	1.69 ± .18	.83 ± .14	.84 ± .07	.58 ± .06
	5:1	26	25.2 ± 3.1	32.2 ± 4.5	37.7 ± 4.1	37.7 ± 2.5	.35 ± .07	.29 ± .06	.41 ± .05	.35 ± .04
	9:1	21	19.5 ± 1.0	22.0 ± 0.9	22.8 ± 0.9	29.0 ± 1.0	.12 ± .02	.09 ± .02	.14 ± .02	.22 ± .01
Inferior lesion	3:1	18	33.5 ± 13.9	49.0 ± 19.2	60.8 ± 17.5	29.5 ± 9.4	2.23 ± .26	1.91 ± .23	1.63 ± .24	.69 ± .23
	5:1	18	14.5 ± 0.5	16.0 ± 0.7	17.2 ± 0.9	15.3 ± 0.5	.66 ± .06	.56 ± .06	.55 ± .05	.14 ± .03
	9:1	14	14.2 ± 0.4	14.5 ± 0.3	15.7 ± 0.2	13.5 ± 0.3	.25 ± .01	.22 ± .01	.22 ± .02	.06 ± .005

* Measurements for 64- and 128-projection imaging protocols, with 50K, 100K, and 200K count studies, were averaged to produce these results for reconstruction methods A, B, C, and D.

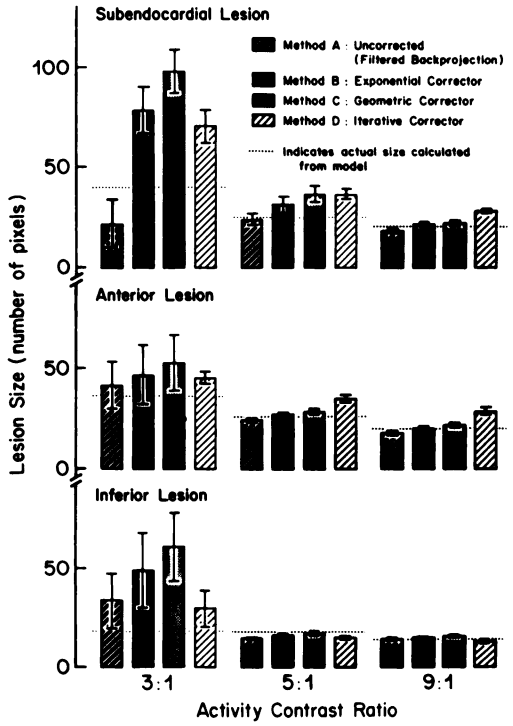

FIG. 4. Lesion size (mean ± standard error) for various reconstruction methods, infarct geometries, and MI-to-background contrast ratios.

some specific characteristics of the imaging system, including Compton-scattered photons and degradation of resolution with source depth. These factors could have been incorporated into the simulations by Monte Carlo methods, and could be studied accurately using physical phantoms. We would expect the four methods tested to be similar in relative response to these degradations, however. The goal of this study was to assess attenuation effects apart from other degrading factors; the mechanism of computer-based simulation enabled us to isolate

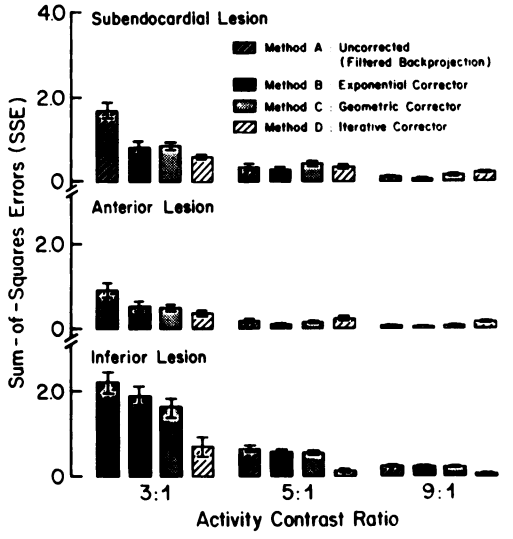

FIG. 5. SSE values (mean ± standard error) for various reconstruction methods, infarct geometries, and MI-to-background contrast ratios.

the attenuation effects and to investigate a large number of study conditions.

The method used for lesion sizing must be considered in interpreting the results of the study. Our approach did not include lesion shape or texture, in keeping with previous studies (*19*,*20*). Manual lesion sizing could have been more accurate than that in our method, but would have been time-consuming and subjective. Alternative automated approaches might use boundary tracking with a dynamic threshold (*28*), or might incorporate expected lesion shape or location (*29*). However, algorithms developed for relatively noise-free data such as those of transmission CT may be ineffective for the poor signal-to-noise ratios found in nuclear medicine images (*30*). The method of this study included image smoothing to control noise, and the threshold approach was objective and computationally simple. In addition, the accuracy measure provided by sum-of-squares error depends both on the normalization scheme used and on the choice of ROI. For consistency we used the same ROI locations and the same normalization for both the lesion sizing and the SSE calculations. Recalculating the SSE values with pixel normalization based on total counts did not change the conclusions of the study. The attenuation-compensation methods we tested did not provide more accurate lesion sizing for all contrast ratios and infarct locations. For MI-to-background ratios of 5:1 or greater, we found no statistically significant differences among the four methods evaluated according to either lesion sizing or SSE. For lower-contrast studies, attenuation compensation was preferable from an SSE standpoint, with the iterative method producing the most accurate reconstructions. Within the framework of the present study, none of the four reconstruction methods tested is clearly superior for Tc-99m PPi myocardial SPECT; in this imaging situation, then, we recommend the reconstruction methods that require less computing time and fewer physical assumptions.

We emphasize that the conclusions of this study do not apply to other methods for attenuation compensation, to other forms of data collection—such as 180° rather than 360° projection data (*31*,*32*)—or to other types of radionuclide study. Also, we did not investigate the effects of camera characteristics or of inaccurately estimated attenuation coefficients on reconstruction accuracy. The approach used in this study, however, would be appropriate for further investigations. Computer-based simulation provides a convenient means to assess the relative performance of different reconstruction methods. For the tuning of a particular method to a particular imaging situation, however, phantom studies are needed. It is also necessary to select evaluation criteria that reflect the nature and purpose of the method being assessed. For our study of Tc-99m PPi myocardial imaging, we believe that lesion sizing is the more important criterion, but in other situations it may be more important to provide accurate reconstruction of activity from an SSE standpoint.

FOOTNOTES

* General Electric Company, Model 400-T.
† Tomographic software, Medical Data Systems, Inc.
‡ Perkin-Elmer 3220 computer.

ACKNOWLEDGMENTS

The authors thank Mr. Gary Smith for assistance with computer programming and Ms. Gayle Blust for secretarial assistance. The research was supported in part by NIH Ischemic Heart Disease SCOR Grant HL-17669.

REFERENCES

1. BUDINGER TF, GULLBERG GT, HUESMAN RH: Emission computed tomography. In *Image reconstruction from projections: Implementation and applications*. GT Herman, Ed. Springer Verlag, 1979, pp 147-246
2. GULLBERG GT: The attenuated Radon transform: Theory and application in medicine and biology. Ph.D. Dissertation, University of California at Berkeley, Lawrence Berkeley Lab. Report LBL-7486, 1979
3. MURPHY PH, THOMPSON WL, MOORE ML, et al: Radionuclide computed tomography of the body using routine radiopharmaticals. I. System characterization. *J Nucl Med* 20:102-107, 1979
4. JASZCZAK RJ, COLEMAN RE, LIM CB: SPECT: Single-photon emission computed tomography. *IEEE Trans Nucl Sci* NS-27:1137-1153, 1980
5. KUHL DE, EDWARDS RQ, RICCI AR, et al: Quantitative section scanning using orthogonal tangent correction. *J Nucl Med* 14:196-200, 1973
6. WALTERS TE, SIMON W, CHESLER DA, et al.: Attenuation correction in gamma emission computed tomography. *J Comput Assist Tomog* 5:89-94, 1981
7. MOORE SC, BRUNELLE JA, KIRSCH CM: An iterative attenuation correction for a single photon, scanning, multi-detector tomographic system. *J Nucl Med* 22:P65, 1981 (abst)
8. SOUSSALINE F, CAO A, LECOQ G: Single photon emission computed tomography using a regularizing iterative method for attenuation correction. In *Proceedings of 7th International Conference on Medical Image Processing*, 1981, (in press)
9. SORENSON JA: Methods for quantitative measurement of radio-activity in vivo by whole-body counting. In *Instrumentation in nuclear medicine*. Vol. 2, GJ Hine and JA Sorenson, Eds. Academic Press, 1974, pp 311-348
10. KAY DB, KEYES JW JR: First order correction for absorption and resolution compensation in radionuclide Fourier tomography. *J Nucl Med* 16:540, 1975 (abst)
11. TRETIAK OJ, DELANEY P: The exponential convolution algorithm for emission computed axial tomography. In *Review of Information Processing in Medical Imaging*. AB Brill and RR Price, Ed. Oak Ridge National Laboratory Report ORNL/BCTIC-2, 1978, pp 266-278
12. CHANG LT: A method for attenuation correction in radionuclide computed tomography. *IEEE Trans Nucl Sci* NS-25:638-643, 1978
13. GULLBERG GT, BUDINGER TF: The use of filtering methods to compensate for constant attenuation in single-photon emission tomography. *Trans Biomed Eng* BME-28:142-157, 1981

14. BUDINGER TF, GULLBERG GT: Three-dimensional reconstruction in nuclear medicine emission imaging. *IEEE Trans Nucl Sci* NS-21:2-20, 1974
15. BUDINGER TF, GULLBERG GT: Transverse section reconstruction of gamma-ray emitting radionuclides in patients. In *Reconstruction tomography in diagnostic radiology and nuclear medicine.* MM Ter-Pogossian et al., Eds. University Park Press, 1977, pp 315-342
16. HERMAN GT, ROWLAND SW: Three methods for reconstructing objects from X-rays: A comparative study. *Comput Graph Image Proc* 2:151-177, 1973
17. BONTE FJ, PARKEY RW, GRAHAM RT, et al: A new method for radionuclide imaging of myocardial infarcts. *Radiology* 110:473-474, 1974
18. PARKEY RW, BONTE FJ, BUJA ML, et al: Myocardial infarct imaging with technetium-99m phosphates. *Semin Nucl Med* 7:15-28, 1977
19. STOKELY EM, BUJA ML, LEWIS SL, et al: Measurement of acute myocardial infarcts in dogs with ^{99m}Tc-stannous pyrophosphate scintigrams. *J Nucl Med* 17:1-5, 1976
20. LEWIS M, BUJA L, SAFFER S, et al: Experimental infarct sizing using computer processing and a three-dimensional model. *Science* 197:167-169, 1977
21. *Radiological Health Handbook*, U.S. Department of Health, Education and Welfare, U.S. Government Printing Office, 1970, pp 66 and 139
22. WILLIAMS DL, RITCHIE JL, HARP GD, et al: Preliminary characterization of a transaxial whole-body single-photon tomograph. In *Proceedings 11th Annual Symposium on the Sharing of Computer Programs and Technology in Nuclear Medicine.* PD Esser, Ed. New York, Society of Nuclear Medicine, 1981, pp 149-166
23. SOUSSALINE FP, TODD-POKROPEK AE, ZUROWSKI S, et al: A rotating conventional gamma camera single-photon tomographic system: Physical characterization. *J Comput Assist Tomogr* 5:551-556, 1981
24. HUESMAN RH, GULLBERG GT, GREENBERG WL, et al: RECLBL Library users manual—Donner algorithms for reconstruction tomography. Lawrence Berkeley Lab. Report PUB-214, 1977
25. SHEPP LA, LOGAN BF: The Fourier reconstruction of a head section. *IEEE Trans Nucl Sci* NS-21:21-43, 1974
26. HERMAN GT: *Image Reconstruction from Projections.* New York, Academic Press, 1980, pp 124-145
27. SIEGEL S: *Nonparametric statistics for the behavioral sciences.* New York, McGraw-Hill, 1956, pp 166-172
28. KELLER JM, EDWARDS FM, RUNDLE R: Automatic outlining of regions of CT scans. *J Comput Assist Tomogr* 5: 240-245, 1981
29. SELFRIDGE PG, PREWITT JMS: Boundary-finding scheme and the problem of complex object localization in computed tomography images. In *SPIE Proceedings on recent and future developments in medical imaging II.* Vol 206, DG Brown and SW Smith, Eds. 1979, pp 193-201
30. TODD-POKROPEK A: Image processing in nuclear medicine. *IEEE Trans Nucl Sci* NS-27:1080-1094, 1980
31. RITCHIE JL, OLSON DO, WILLIAMS DL, et al: Transaxial computed tomography with ^{201}Tl in patients with prior myocardial infarction. *J Nucl Med* 22:P11, 1981 (abst)
32. BESOZZI MC, RIZI HR, ROGERS WL, et al: Rotating gamma camera ECT of Tl-201 in the human heart. *J Nucl Med* 22:P11, 1981 (abst)